Proceedings of the Mustansiriyah International Conference on Applied Physics (MICAP-2021)

Preparation of High-Performance Room Temperature ZnO Nanostructures Gas Sensor

Haitham M. Mikhlif[a,*], Mohammed O. Dawood[a], Oday M. Abdulmunem[a] and Mohanad K. Mejbel[b]

[a] *Department of Physics, College of Science, Mustansiriyah University, Palestine St., 10052, Baghdad, Iraq*
[b] *Materials Techniques Engineering Department, Engineering Technical College-Baghdad, Middle Technical University (MTU), Baghdad, Iraq*

Doi: 10.12693/APhysPolA.140.320 *e-mail: haitham.mikhlif@uomustansiriyah.edu.iq

Zinc oxide (ZnO) nanostructures were deposited on glass substrates by physical vapor deposition technique. To improve the crystallinity of ZnO, oxidation treatment was conducted at 400° for 1 h in an atmospheric environment. The films characteristics of the films were examined by X-ray diffraction, ultraviolet–visible spectroscopy, atomic force microscopy, and scanning electron microscopy. The X-ray diffraction results illustrated that the deposited films have a polycrystalline hexagonal structure. The ultraviolet-visible spectrum showed that the transmittance of the ZnO film has an energy gap of about 3.225 eV. The atomic force microscopy images indicated that the films have good homogeneity, and the scanning electron microscopy images reveal that they consist of spherical nanosized grains with a granular surface. The ZnO films revealed good sensing performance to acetone and ethanol gases at an operating temperature of 25°C with suitable recovery and response times. The sensitivity measured by homemade gas sensor system was approximately 21.39, 29.63, 23.8% for acetone gas, and 15.96, 21.28, 20.97% for ethanol gas, at 125, 250, 500 ppm concentrations, respectively.

topics: polycrystalline crystal, ZnO nanostructure, physical vapor deposition, gas sensor

1. Introduction

In the last decade, ZnO nanostructures have become worthwhile because of their significant physical and chemical properties as well as various technological applications. ZnO is an n-type II–VI group compound with a hexagonal crystalline (wurtzite) structure with a direct energy gap of 3.37 eV at room temperature and a high exciton voltage bonding of 60 meV [1–3]. ZnO nanocrystalline is essential for many applications in electrochemical, electromechanical, electronic and optoelectronic devices [4–8] such as solar cells [9–12], ultraviolet (UV) lasers [13, 14], field emission devices [15–17], light-emitting diodes [18], nanosensors [19–21] and nano-piezotronics [22–24].

Zinc oxide thin films are grown by chemical and physical techniques. Physical methods such as evaporation by electron beam epitaxy technique [25], pulsed-laser evaporation [26], reactive magnetron sputtering [27], physical vapor deposition (PVD) [28] etc. allow the production of high quality polycrystalline–crystalline nanostructures with homogeneous surface, high efficiency and safe. There are a variety of chemical methods used to deposit ZnO films, for example, chemical bath deposition (CBD) [29], electrode position [30], thermal evaporation [31], spray pyrolysis [32] and multi precipitation method [33]. The zinc oxide thin film has a high electrical resistance when annealing is done in atmosphere air because of oxygen adsorption/desorption process of surface, thus, electrical resistance of the sensing material changes [34].

Acetone and ethanol gases are usually classified as volatile organic compound (VOC) [35]. Acetone evaporates when exposed to the atmosphere and exhibits slight toxicity in normal use. There is also some evidence of chronic health effects if no precautions are followed. Although ethanol is a common material used, it is also a toxic chemical and highly flammable. In alcoholic beverages, for example, the consumption of ethanol alone can cause coma and death. Therefore, it must be treated with great care at home or in the work.

According to the above, gas sensors should be small in size, quick reacting, have a long lifetime and good sensitivity to detect acetone and ethanol gases in low concentrations. The particle size and surface morphology are the main variables relevant for the gas sensing properties for the metal oxide

gas sensors [36]. The aim of this study is to use PVD technique to grow polycrystalline–crystal ZnO thin films for acetone and ethanol gas detection by a homemade gas sensing system prepared at room temperature (25°C).

2. Materials and methods

Edward 306 (UK) system was used for depositing zinc powder of 99.999% high purity from Palintest Ltd, UK. The pressure was 2×10^{-5} mbar, and a 2×2 cm^2 glass substrates were used for depositing at room temperature. Glass substrates were ultrasonically cleaned, vibrated both in a steel tank with acetone and in ethanol for 10 min, and rinsed off with distilled water at each step. Finally, the glass substrates were dried with a gas flow of nitrogen. The obtained distance between the molybdenum boat containing Zn powder and the substrate was 100 mm. After the deposition process, the samples were oxidized at $T = 400$°C for 1 h in a furnace with an air atmosphere ensuring that temperature did not exceed 400°C, which would lead to an undesirable increase in the crystal size. The samples were then left to be cooled down to room temperature [37–39]. The zinc oxide deposited films were examined via FESEM. The atomic force microscopy (AFM) scans were used to study morphology and average roughness of the prepared ZnO thin films. The sensing parameters: dynamic resistance, response time, and recovery time were tested by a laboratory testing system, as shown in Fig. 1. The zinc oxide films were exposed to many concentrations of acetone gas and ethanol gas at room temperature.

The system unit of gas sensor testing consists of a cylindrical stainless–steel chamber with vacuum-tight of a 20 cm diameter and a 16 cm height, having a volume of 5540 cm^3. In addition, the electrodes needles were used to connect to the samples by flexible contact, as these needles contain a spring. The test chamber had a sealed O-ring as a removable bottom base, and it has an inlet for allowing the test gas to flow in, and the air valve for allowing the atmospheric air to go in after evacuation. Acetone gas was injected at various concentrations in the closed sealed chamber by opening the inlet valve, and air is pumped in the chamber. The same procedure was repeated for ethanol and all gas sensor tests are done at room temperature.

3. Results and discussions

3.1. Structural properties

Figure 2 shows the X-ray difraction (XRD) pattern of ZnO thin film prepared by the PVD technique which confirms the hexagonal (wurtzite) structure, and it is in agreement with JCPDS card No. 00-036-1451. The peak reflection $2\theta = 34.5°$ indicates polycrystalline–crystalline diffraction at

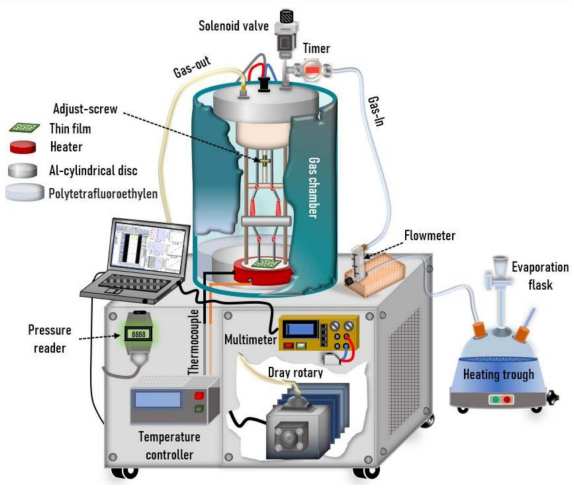

Fig. 1. Home-made gas sensor testing system.

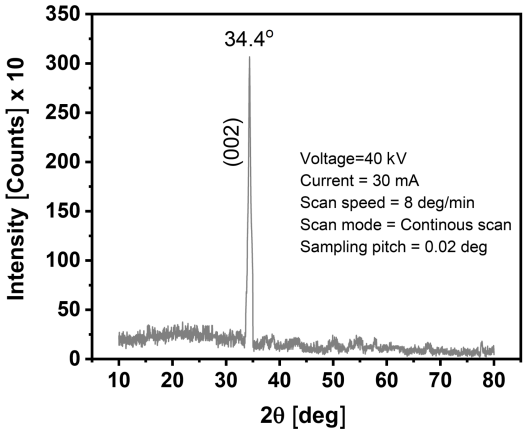

Fig. 2. The XRD pattern of ZnO thin film prepared by the PVD technique.

the (002) plane. The intensity and full-width half-maximum of the (002) plane shows that the crystallite size D of zinc oxide nanostructure film is 39.61 nm. It is calculated by the Scherrer equation, i.e.,

$$D = \frac{K\lambda}{\beta \cos(\theta)}, \tag{1}$$

where $\lambda = 1.54056$ Å, θ is the diffraction plane angle, β is defined as the half width at half maximum (FWHM) of the main peak and it equals to 0.210°. When K is constant, D depends on the nature of material (in our experiment $K = 0.9$).

The microstrain ε was evaluated during the growth of the nanostructure film. The value of ε for the ZnO film is equal to 9.149×10^{-4}/line^2. It is determined as follows

$$\varepsilon = \frac{\beta \cos(\theta)}{4}, \tag{2}$$

where δ is the density of dislocation that indicates a crystal imperfection related to the lattice distortion.

The dislocation density δ for the ZnO nanostructure is 6.372×10^{14} m^{-2} and determined as

$$\delta = \frac{1}{D^2}. \tag{3}$$

The structural variables of ZnO film in Fig. 2 is also reported in [39].

3.2. Optical properties

The spectral transmittance of the ZnO thin film oxide at 400° was recorded for the range of wavelengths 300–900 nm using the ultraviolet–visible (UV–VIS) spectrometer, as illustrated in Fig. 3a. The result shows that the optical transmittance increases with increasing the incident wavelength and is grater than 90% in the 400–900 nm region because of homogeneous crystallinity of the films. The absorption coefficient (α) can be determined from the spectral transmittance by [40]

$$\alpha(\lambda) = \frac{1}{d} \ln\left(\frac{1}{T}\right), \tag{4}$$

where d is the thickness, and T is the percentage transmittance. The calculated value of absorption coefficient α was greater than 10^4 cm^{-1}, which means that the electronic transitions are direct.

In Fig. 3b, the absorption coefficient α as a function of incident wavelength λ for the ZnO film deposited on glass substrates and oxidation at 400°C is illustrated in Fig. 4. The absorption coefficient decreases sharply in the UV and VIS regions and then gradually decreases in the VIS region as it is proportional to the transmittance. These decreases may be attributed to the low roughness and incident light scattering effect. The increase in the α coefficient indicates a high probability of direct electronic transitions.

At the absorptance edge and with high photons absorption potential, the absorption coefficient α increases in the high energies' direction. The energy gap value E_g of the thin film may be determined using [41]

$$\alpha h\nu = A\left(h\nu - E_g\right)^n, \tag{5}$$

where A is an independent constant, E_g is the energy gap, $h\nu$ is the incident photon energy, and α is the absorptance coefficient. Figure 3c shows the spectral energy gap of ZnO film deposited by PVD technique. The value of E_g may be determined by linear extrapolation of $(\alpha h\nu)^2$. It is found that $E_g = 3.225$ eV which is in agreement with Malek et al. [42] and Zaier et al. [43].

The surface morphology images of zinc oxide films with the scanning electron microscopy (SEM) are illustrated in Fig. 4. The surface of the ZnO film in Fig. 4a consists of spherical nanometric grains of almost regular size covering the substrate. A high homogeneity of the surface can also be observed. The average grain size is approximately 34.44 nm. In the SEM cross-section of ZnO deposited films(see Fig. 4b) one can see that the larger size of particles seems bright. This may be due to the agglomeration of nanoparticles that scatter the incident electrons in the same phase. The grain size that observed from SEM analysis seems smaller than the crystallite size obtained from the XRD analysis by using Scherrer's equation. In fact, these results agree with Ayouchi et al. [44].

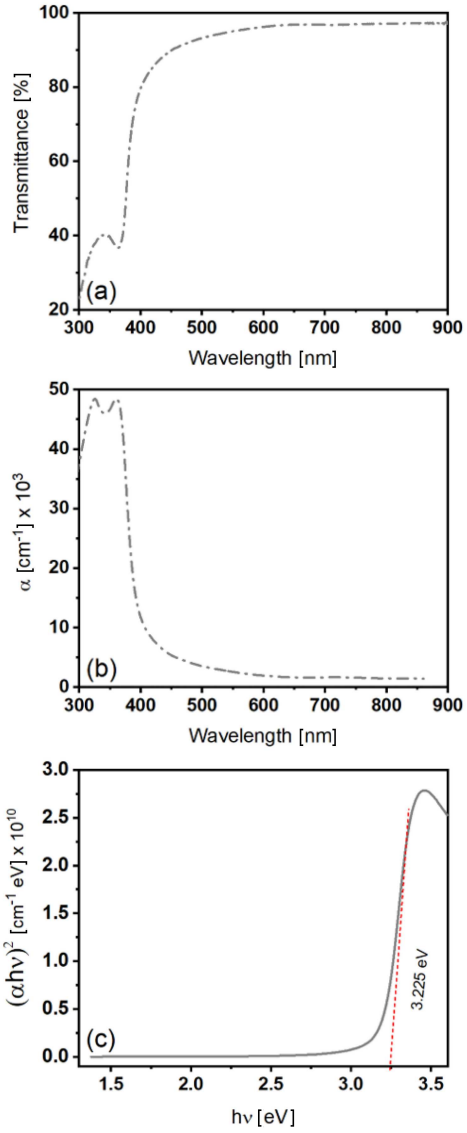

Fig. 3. Illustration of (a) the spectral transmittance T, (b) the absorption coefficients α as a function of the incident wavelength λ and (c) a spectral energy gap E_g of ZnO film deposited by PVD technique.

Figure 4c and d represents, respectively, the 2D and 3D AFM images of ZnO nanostructure film with a 10×10 μm^2 area. The obtained results reveal that the grain size is approximately 34 nm which is in line with the SEM analyses. The average roughness of 5.091 nm indicates a good homogeneity. Moreover, the grain size affects the resistivity, so that the conductive properties of the films mightily depend on the character of the material morphology [45, 46].

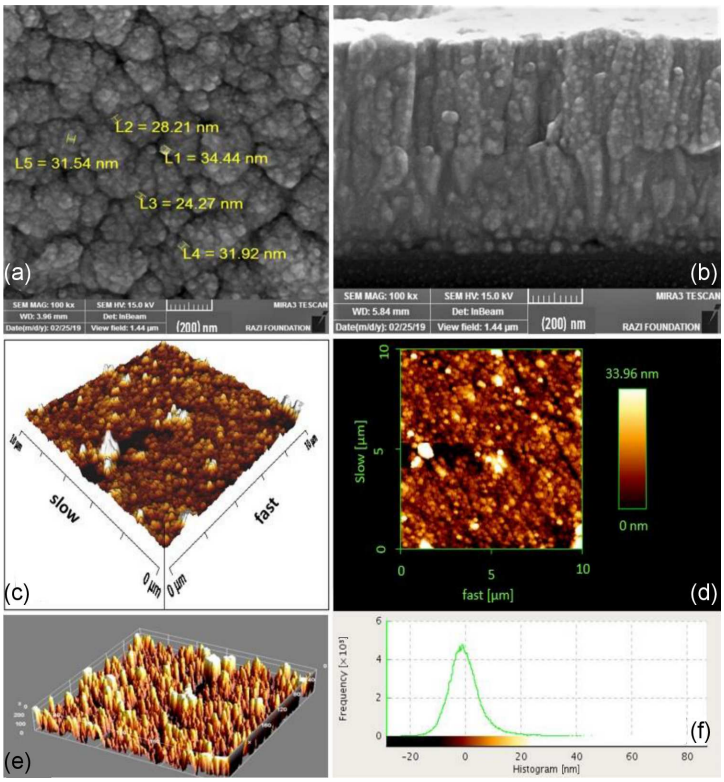

Fig. 4. The morphology images in (a, b), the cross and surface view by SEM scanning in two and three dimensions (c)–(e), the histogram diagram by AFM of ZnO film deposited by PVD technique (f).

Concerning the gas sensing applications, semiconductor metal oxides (SMO) have a well-known characteristic that their surface may absorb the oxygen molecules when exposed to an oxidizing gas. For example, the atmosphere air has the 22% oxygen. For the ethanol gas sensing by oxygen absorption and determining the electrical transport properties of the ZnO nanostructures, it turns out that the absorption of the oxygen ions decrease the conductance of ZnO and removes the conducted electrons [47]. Further, the atmospheric–oxygen interaction causes absorption of the ions as atomic (O^-, O^2) and molecular (O^{2-}) species [48].

The concentration c [ppm] of acetone and ethanol vapor can be expressed by [36, 37, 48]

$$\frac{V_{\text{target gas}}}{V_{\text{test chamber}}} = c \times 10^{-6}, \tag{6}$$

where the volumes $V_{\text{target gas}}$ and $V_{\text{test chamber}}$ are typicaly given in cm.

Figure 5a and b shows the change in dynamic resistance with a production time of ZnO films by PVD technique exposed to various concentrations (125, 250, 500 ppm) of acetone and ethanol gases at room temperature. The gas sensor resistance of the samples was low and attributed to the increased sensitivity due to the increased surface area and thus lower resistance. The resistance of the ZnO sensor gradually increases with time as concentrations of both gases increase. In the case of the prepared ZnO thin films, they reveal n-type semiconductor nature (i.e., increasing the resistance when exposed to the oxidizing gas). So in fact, the resistance of the ZnO film is increased by increasing the acetone concentrations first and then ethanol secondly inside the chamber [49]. This behaviour can be explained as follows: the electrons are taken from the ionized donors in the conduction band and the majority of charge carriers' concentration will increase at the gas–solid interface. This leads to a higher potential barrier and, as a result, to a decrease of the ZnO surface oxygen ions density. The potential barrier and the depletion layer provide the highest electrical resistivity that depends significantly on the concentration of the oxygen ions absorbed on the surface. The pumping of either acetone or ethanol gas to the ambient chamber varies the concentration of the ions and the resistance increases [47].

The disposal of the oxygen vacancies during the annealing process is due to dissociative O_2 adsorption and uptake of oxygen to the subsurface. Interstitial oxygen diffusion leads to spontaneous annihilation between the oxygen vacancy and the interstitial oxygen in the zinc oxide substrate, as well as enhances the zinc oxide substrate resistivity. The uptake of oxygen into zinc oxide substrate, followed by teh elimination of the vacancies, was confirmed by a change in color of the zinc oxide substrate with annealing [34]. ZnO substrate shows a yellow tinge which is attributed to oxygen vacancies and it has been found that the oxygen vacancies decrease with the annealing of zinc oxide films.

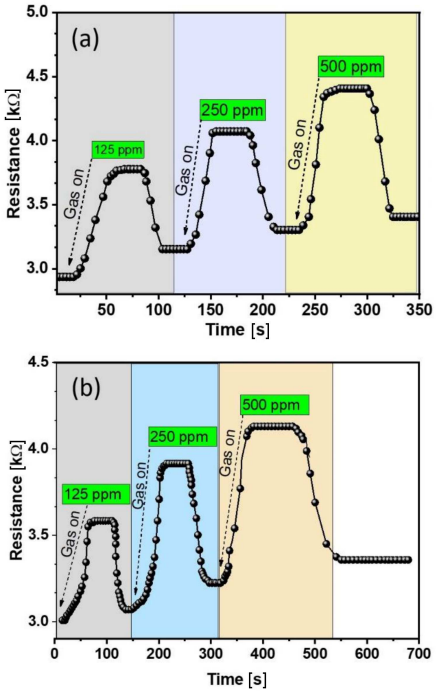

Fig. 5. The change in dynamic resistance versus production time of ZnO films with (a) acetone and (b) ethanol.

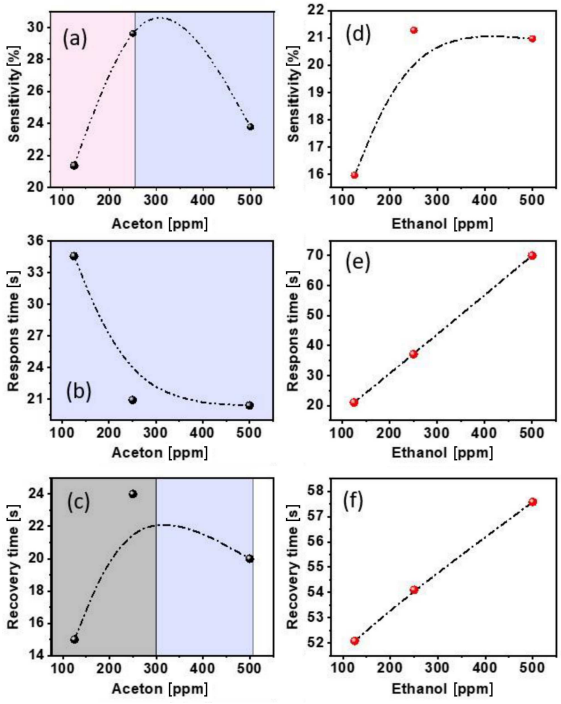

Fig. 6. (a, b) The sensitivity, (c, d) the response time and (e, f) the recovery time, respectively, for acetone and ethanol gas concentrations.

The gas sensor sensitivity is measured accordingly [36–38]

$$S = \frac{R_g - R_a}{R_g} \times 100\%, \tag{7}$$

where S is the sensitivity of the sensor, R_a is the resistance of the sensor in air, and R_g is the resistance of the sensor in a gas.

Figure 6a and d illustrates the sensitivity percentage of the ZnO nanostructure thin film via gas concentrations [ppm] for acetone and ethanol gases. The measured sensitivity is approximately 21.39, 29.63, 23.8% for acetone gas, and 15.96, 21.28, 20.97% for ethanol gas at 125, 250, 500 ppm concentrations, respectively. The two gases were operated at room temperature. The sensitivity percentage is calculated assuming the interaction between target gas and the surface area of the gas sensor. AFM measurements show a larger surface area to nanostructure films which confirm the interaction activity between the sensor surface and the adsorbed acetone and ethanol gases, i.e., higher sensitivity percentage for the gas sensor. The ZnO film sensitivity percentage depends significantly on the changes in the adsorbed oxygen ions concentration located on the ZnO film surface. This agrees with Ge et al. [50].

Response time is defined as the time interval over which the resistance of the sensor material reaches a particular percentage of the ultimate value (usually 90%) when the sensing material is exposed to the full concentration of the target gas. The short response time in a lot of applications such as detection of the flammable gases [35, 36] is very desired.

Figures 6b and e shows the response time of ZnO samples as a function of acetone and ethanol concentrations. The measured responses time were approximately 34.59, 20.93, 20.4 s for acetone gas, and 52.08, 54.1, 57.58 s for ethanol gas at 125, 250, 500 ppm concentrations, respectively. The two gases were operated at room temperature. The sensor response magnitude for the two gases increases with increasing the concentrations of the two gases. The results demonstrate that the sensor response time is stable, and they are in line with Hsueh et al. [51].

The ions of the adsorbed oxygen in a 2 electron valence state are accountable for acetone gas and ethanol gas sensing. The contributory oxygen forms in acetone and ethanol sensing are either O^{2-} or O_2^{2-}. However, the last form is less probable when taking into account the thermal dismantling of oxygen molecules on a ZnO film surface, which is widely accepted. The experiment revealed that the desorption/adsorption of the ions of adsorbed oxygen are reversible on the zinc oxide film surface, whereas the adsorbed oxygen is partially combined into the implied subsurface and so the ZnO film resistance depends on annealing process [34].

Yang et al. [52] explained the oxidation mechanism of ethanol gas on an oxygen-adsorbed zinc oxide surface and revealed that the oxidation of ethanol gas to acetaldehyde is likely only on the zinc oxide film surface with thermal dissociation of the atomic oxygen. Thus, the reaction rate of the ethanol gas depends on the concentration of adsorbed oxygen ions. In this study, the behaviour of

surface oxygen (desorption, adsorption, interdiffusion, decomposition, ionization, and deionization) controls the sensing properties of ZnO sensor. The recovery time for the gas sensor should be as short as possible so that it is ready for the next detection [35, 36].

Figure 6c and f represents the recovery time for acetone and ethanol gases. This recovery time can be estimated directly from the change in the dynamic resistance of ZnO films and plotted as a function of the gas concentrations [ppm]. The measured recovery times are approximately 15, 24, 20 s for acetone gas, and 21, 37.1, 70 s for ethanol gas at 125, 250, 500 ppm concentrations, respectively. Both gases were operated at room temperature. note that the recovery times vary with increasing concentration of two gases which is an expected feature in sensing applications.

4. Conclusions

ZnO nanostructured thin films were successfully prepared using PVD technique and measured by a locally manufactured system for gaseous sensors applications. The films were oxidized at 400°C for 1 h in the atmospheric air. The structural and morphological analysis revealed that the nanostructures have a hexagonal (wurtzite) nanostructure with polycrystalline crystal diffraction at (002) orientation and a crystallite size of ≈ 39.6 nm. The optical band gap for ZnO was 3.225 eV. Surface morphological investigations reported a granule size of ~ 40 nm. The results of ZnO thin films revealed to be suitable for optoelectronic implementations. These ZnO nanostructured samples were tested at room temperature via acetone and ethanol gases, showing fast recovery-response time, and excellent sensitivity. The highest sensitivity percentage value is approximately 30% for acetone gas and 22% for ethanol gas at 250 ppm concentrations when the two gases operated at room temperature. The best response time at 500 ppm concentration was 20.4 s for acetone and 52 s for ethanol. In turn, the best recovery time at 125 ppm concentration was 15 s for acetone and 21 s for ethanol.

The atomic arrangement and accurate stoichiometry of the zinc oxide polycrystalline–crystalline substrate enabled good analysis of acetone gas and ethanol gas sensing mechanism. The ZnO substrate tends to show high resistance with annealing in air. This behaviour was due to the adsorption/desorption of surface oxygen types. The acetone sensing sensitivity was larger with higher resistance of the zinc oxide substrate. This can be noticed through the relationship between the charge carrier's concentration governed by oxygen ionosorption and the sensitivity of the sensor. This study shows that a ZnO polycrystalline crystal is appropriate for understanding the gas sensing mechanism, which may be provided with best ideas into the design of new gas sensors manufactured from semiconductor materials.

Acknowledgments

The authors would like to express their gratitude and acknowledge to the Department of Physics, College of Science at Mustansiriyah University for using the advanced material Lab. (www.uomustansiriyah.edu.iq)

References

[1] H. Morkoç, Ü. Özgür, *Zinc Oxide: Fundamentals, Materials and Device Technology*, Wiley, 2008.

[2] C. Klingshirn, *ChemPhysChem* **8**, 6 (2007).

[3] D.P. Norton, Y.W. Heo, M.P. Ivill, K. Ip, S.J. Pearton, M.F. Chisholm, T. Steiner, *Mater. Today* **7**, 6 (2004).

[4] Z.L. Wang, *ACS Nano* **2**, 10 (2008).

[5] G.C. Yi, C. Wang, W. Il Park, *Semicond. Sci. Technol.* **20**, 4 (2005).

[6] Z.L. Wang, *J. Nanosci. Nanotechnol.* **8**, 1 (2008).

[7] Z.L. Wang, *Mater. Sci. Eng. R Rep.* **64**, 3 (2009).

[8] Z.L. Wang, *Chin. Sci. Bull.* **54**, 22 (2009).

[9] M. Law, L.E. Greene, J.C. Johnson, R. Saykally, P. Yang, *Nat. Mater.* **4**, 6 (2005).

[10] C. Lévy-Clément, R. Tena-Zaera, M.A. Ryan, A. Katty, G. Hodes, *Adv. Mater.* **17**, 12 (2005).

[11] B. Weintraub, Y. Wei, Z.L. Wang, *Angew. Chem.* **121**, 9143 (2009).

[12] Y. Wei, C. Xu, S. Xu, C. Li, W. Wu, Z.L. Wang, *Nano Lett.* **10**, 6 (2010).

[13] K. Govender, D.S. Boyle, P. O'Brien, D. Binks, D. West, D. Coleman, *Adv. Mater.* **14**, 17 (2002).

[14] M.H. Huang, S. Mao, H. Feick, H. Yan, Y. Wu, H. Kind, E. Weber, R. Russo, P. Yang, *Science* **292**, 5523 (2001).

[15] D.S. Mao, X. Wang, W. Li, X.H. Liu, Q. Li, J.F. Xu, *J. Vac. Sci. Technol. B* **20**, 1 (2002).

[16] Y.W. Zhu, Hongzhou Zhang, Xiaoming Sun, Shi-Qing Feng, J. Xu, Q. Zhao, Baixiang Xiang, Rongming Wang, Dapeng Yu, *Appl. Phys. Lett.* **83**, 1 (2003).

[17] W.Z. Wang, Baoqing Zeng, Jian Yang, Bed Poudel, Jian Yu Huang, M.J. Naughton, Z.F. Ren, *Adv. Mater.* **18**, 24 (2006).

[18] W. Il Park, G. Yi, *Adv. Mater.* **16**, 1 (2004).

[19] T.-Y. Wei, P.-H. Yeh, S.-Y. Lu, Z.L. Wang, *J. Am. Chem. Soc.* **131**, 48 (2009).

[20] P. Yeh, Z. Li, Z.L. Wang, *Adv. Mater.* **21**, 48 (2009).

[21] J. Zhou, Yudong Gu, Youfan Hu, Wenjie Mai, Ping-Hung Yeh, Gang Bao, A.K. Sood, D.L. Polla, Zhong Lin Wang, *Appl. Phys. Lett.* **94**, 191103 (2009).

[22] Z.L. Wang, J. Song, *Science* **312**, 5771 (2006).

[23] X. Wang, J. Song, J. Liu, Z.L. Wang, *Science* **316**, 5821 (2007).

[24] R. Yang, Y. Qin, L. Dai, Z.L. Wang, *Nat. Nanotechnol.* **4**, 1 (2009).

[25] R. Al Asmar, D. Zaouk, P. Bahouth, J. Podleki, A. Foucaran, *Microelectron. Eng.* **83**, 3 (2006).

[26] X.W. Sun, H.S. Kwok, *J. Appl. Phys.* **86**, 1 (1999).

[27] E.-G. Fu, D.-M. Zhuang, G. Zhang, W.F. Yang, M. Zhao, *Appl. Surf. Sci.* **217**, 1 (2003).

[28] G. Jimenez-Cadena, E. Comini, M. Ferroni, A. Vomiero, G. Sberveglieri, *Mater. Chem. Phys.* **124**, 1 (2010).

[29] S.H. Chiu, J.C.A. Huang, *J. Non-Cryst. Solids* **358**, 17 (2012).

[30] Y.-F. Gao, M. Nagai, Y. Masuda, F. Sato, K. Koumoto, *J. Cryst. Growth* **286**, 2 (2006).

[31] R. Yi, H. Zhou, N. Zhang, G. Qiu, X. Liu, *J. Alloys Compd.* **479**, 1 (2009).

[32] Z. Sofiani, B. Derkowska, P. Dalasiński et al., *Opt. Commun.* **267**, 433 (2006).

[33] R. Kripal, A.K. Gupta, R.K. Srivastava, S.K. Mishra, *Spectrochim. Acta A* **79**, 5 (2011).

[34] T.T. Suzuki, T. Ohgaki, Y. Adachi, I. Sakaguchi, M. Nakamura, H. Ohashi, A. Aimi, K. Fujimoto, *ACS Omega* **5**, 33 (2020).

[35] G.S. Thakor, Ning Zhang, R.M. Santos, *Clean Technol.* **3**, 519 (2021).

[36] A. Fajar, Gunawan Gunawan, E. Kartini, H. Mugirahardjo, M. Ihsan, *Atom Indonesia* **36**, 3 (2011).

[37] A. Nuraini, I. Noor Mazni, D.M. Nuruzzaman, *Malays. J. Anal. Sci.* **22**, 6 (2018).

[38] O.M. Abdulmunem, M.J. Ali, E.S. Hassan, *Opt. Mater.* **109**, 110374, 2020.

[39] S. Nallusamy, B. Deenadhaya, R. KalpoondiS, J. Bosco Balaguru Rayappan, *J. Appl. Sci.* **12**, 16 (2012).

[40] S.J. Mezher, M.O. Dawood, O.M. Abdulmunem, M.K. Mejbel, *Vacuum* **172**, 109074 (2020).

[41] S.J. Mezher, M.O. Dawood, A.A. Beddai, M.K. Mejbel, *Mater. Technol.* **35**, 60 (2019).

[42] M.F. Malek, M.H. Mamat, M.Z. Musa et al., *J. Alloys Compd.* **610**, 575 (2014).

[43] A. Zaier, A. Meftah, A.Y. Jaber, A.A. Abdelaziz, M.S. Aida, *J. King Saud Univ.-Sci.* **27**, 4 (2015).

[44] R. Ayouchi, F. Martin, D. Leinen, J.R. Ramos-Barrado, *J. Cryst. Growth* **247**, 497 (2003).

[45] R. Yogamalar, R. Srinivasan, A. Vinu, K. Ariga, A.C. Bose, *Solid State Commun.* **149**, 43 (2009).

[46] A.G.S. Kumar, L. Obulapathi, T.S. Sarmash, D. Jhansi Rani, M. Maddaiah, T. Subba Rao, K. Asokan, *JOM* **67**, 4 (2015).

[47] S. Maeng, S.W. Kim, D.H. Lee, S.E. Moon, K.C. Kim, A. Maiti, *ACS Appl. Mater. Interfaces* **6**, 1 (2014).

[48] N. Barsan, U. Weimar, *J. Electroceram.* **7**, 3 (2001).

[49] R. Pandeeswari, B.G. Jeyaprakash, *Sens. Actuat. B Chem.* **195**, 206 (2014)

[50] C. Ge, C. Xie, and S. Cai, *Mater. Sci. Eng. B* **137**, 1 (2007).

[51] T.J. Hsueh, C.-L. Hsu, *Sens. Actuators B Chem.* **131**, 2 (2008).

[52] T. Yang, Y. Liu, W. Jin, Y. Han, S. Yang, W. Chen, *ACS Sensors* **2**, 7 (2017).